CONCURRENT ENGINEERING: Research and Applications

CAD-Based Shape Optimization Using a Meshfree Method

Iulian Grindeanu, Nam H. Kim, Kyung K. Choi* and Jiun S. Chen

*Center for Computer-Aided Design and Department of Mechanical Engineering, The University of Iowa,
Iowa City, IA 52242, USA*

Received 28 April 2001

Abstract: A shape design sensitivity analysis and optimization procedure is proposed using a meshfree method. A CAD tool connection is established to facilitate the seamless integration of structural modeling, simulation, and design optimization. A new CAD-based method for design velocity computation is proposed, applicable to both the meshfree method and the finite element method. A shape design variable can be chosen among the geometric parameters defined in the CAD model in order to support a concurrent engineering environment. A new CAD-based method for updating the discrete model is proposed, such that the meshfree model is automatically updated in a continuous and consistent way during design optimization. The proposed method is applied to 2D and 3D linear elastic problems, as well as to a large deformation hyperelastic problem.

Key Words: CAD-based design, design sensitivity analysis, design optimization, meshfree method.

1. Introduction

Recent advances in the field of shape design optimization make it possible to develop an automated, CAD-based product design process. In order to apply shape optimization to industrial problems, the following methods must be developed: geometry-based design parameterization, automatic mesh generation, design velocity computation, and seamless integration with a CAD tool. A seamless integration between a CAD tool, simulation, design sensitivity analysis, and optimization is established in the Pro/ENGINEER environment [1], which provides access to a model database through a set of functions organized in Pro/TOOLKIT and Pro/DEVELOP libraries. These libraries allow users to add functionality to Pro/ENGINEER as well as the ability to integrate the resulting application. A graphical user interface is developed under the Pro/ENGINEER's menu system.

In the shape optimization, the design velocity is important information for calculating sensitivity and updating the discrete model. A number of design velocity computation methods have previously been proposed: the finite difference method [2,3], the isoparametric mapping method [4–6], the boundary displacement method [7], the fictitious load method [8,9], and a combination of the isoparametric mapping and boundary displacement method [5,10]. Hardee et al. [3] propose updating the discrete model using a linear design velocity field obtained from the finite difference technique, while the CAD model is updated by automatic parameter regeneration. With a small shape-changing problem the difference between two updating processes can be ignored. As the design change increases, however, nonlinear effects become dominant such that a node on the boundary surface of the initial design may not remain on the boundary of the perturbed design, causing inconsistency between the discrete and CAD model.

In this paper, a new hierarchical boundary displacement method is proposed. The coordinates of the perturbed points on the edges are computed by isoparametric mapping, using the 1D parameters from the initial design. Points on the boundary surfaces are updated using a 2D boundary displacement method in the surface parametric space. The points in the interior of the structure are updated using a 3D boundary displacement method. This method is capable of maintaining consistency between the discrete and CAD model throughout the design optimization process. More specifically, points that were initially on an edge will remain on that edge, points that were initially on a surface will remain on that surface. Current limitation of the procedure proposed above is that the design changes are in such a way that underlying topology of the CAD model is not changed, i.e., the number and connectivity of curves and surfaces are not changed due to design changes.

*Author to whom correspondence should be addressed.
E-mail: kkchoi@ccad.uniowa.edu

1063-293X/02/01 0055–12 $10.00/0 DOI: 10.1106/106329302024056

Hardee's development of a CAD-based design optimization process is based on the finite element method. However, the mesh quality generated from a CAD tool is not good enough for FEA purposes. In addition, conventional mesh distortion still takes place during the shape optimization process. In this paper, a meshfree method is used as a simulation tool, such that solution accuracy and mesh quality problems in the CAD tool can be resolved. Meshfree methods [11] require a set of nodes (particles) to be defined in the domain, but do not require any pre-specified connectivity between nodes, or any locally regular topological structure as is required in traditional meshing. These particles can be automatically generated using a variety of methods that have been borrowed from traditional FEA. An important advantage of the meshfree method is the continuity of the approximation on internal boundaries. The most an FEA solution can exhibit is C^1-continuity properties across the element boundaries, while a meshfree solution may exhibit any degree of regularity necessary for a given problem.

2. Reproducing the Kernel Particle Method

Although the meshfree method requires a set of particles to be defined in the domain, it does not require a locally regular topological structure (connectivity) that is used in traditional meshing for the finite element or finite difference method. With the meshfree approach, the Galerkin procedure is employed in a similar way to the finite element method, but the finite dimensional solution space and trial space are constructed using meshfree shape functions as the basis functions. The shape function associated with each particle has a compact support, and its construction depends on the geometric relations between the surrounding particles and the boundary of the physical domain. Starting from a CAD model, the generation of particle points used in the meshfree method is automated where a boundary representation of the model is available. Topologically complex domains can be discretized automatically with tetrahedral (or triangular) finite elements. Typically, finite element results based on these elements have a low rate of accuracy. However, the decomposition of the physical domain using tetrahedrons or triangles can be successfully used in the meshfree method for numerical integration purposes.

In Figure 1, the discretization process is explained. Starting from a CAD model, a set of particles is generated in the domain, and a finite support is associated with each particle. Meshfree shape functions can be constructed at any point $\boldsymbol{X}$ in the domain, using the formula from Liu [12]

$$\begin{aligned}\Psi_I(X) &= C(\boldsymbol{X}, \boldsymbol{X} - \boldsymbol{X}_I)\Phi_a(\boldsymbol{X} - \boldsymbol{X}_I)\Delta W_I \\ &= \boldsymbol{H}^T(\boldsymbol{X} - \boldsymbol{X}_I)\boldsymbol{M}^{-1}(\boldsymbol{X})\boldsymbol{H}(0)\Phi_{a_I}(\boldsymbol{X} - \boldsymbol{X}_I)\Delta W_I\end{aligned} \tag{1}$$

where $C(\boldsymbol{X}, \boldsymbol{X}{-}\boldsymbol{X}_I) = \boldsymbol{H}(\boldsymbol{X}{-}\boldsymbol{X}_I)^T M^{-1}(\boldsymbol{X})\boldsymbol{H}(0)$ is a correction function, $\boldsymbol{H}(\boldsymbol{X}{-}\boldsymbol{X}_I) = \{1,\ X{-}X_I,\ Y{-}Y_I, \ldots, (Y{-}Y_I)^n\}^T$ is a vector that contains monomials up to degree n, $\Phi_{a_I}(\boldsymbol{X} - \boldsymbol{X}_I)$ is the window function associated with the particle I with support size a_I, and ΔW_I is the weight associated with each particle. The weight function (also called the window, or the kernel function) is obtained by extension to 2D or 3D of a 1D cubic spline function as

$$\begin{aligned}\Phi_{a_I}(\boldsymbol{X} - \boldsymbol{X}_I) &= w\left(\frac{\|\boldsymbol{X} - \boldsymbol{X}_I\|}{a_I}\right) \text{ or} \\ \Phi_{a_I}(\boldsymbol{X} - \boldsymbol{X}_I) &= w\left(\frac{|X - X_I|}{a_I}\right) \cdot w\left(\frac{|Y - Y_I|}{a_I}\right)\end{aligned} \tag{2}$$

where

$$w(\alpha) = \begin{cases} 2/3 - 4\alpha^2 + 4\alpha^3 & \text{for } |\alpha| \le 1/2 \\ 4/3 - 4\alpha + 4\alpha^2 - 4\alpha^3/3 & \text{for } 1/2 < |\alpha| \le 1 \\ 0 & \text{for } |\alpha| > 1 \end{cases} \tag{3}$$

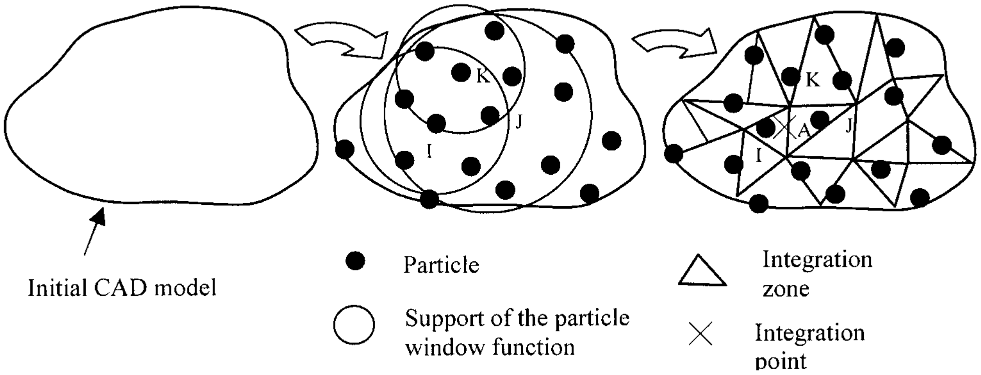

Figure 1. The meshfree discretization process.

The moment matrix $\boldsymbol{M}$ is computed from the following relation:

$$\boldsymbol{M}(\boldsymbol{X}) = \sum_{J=1}^{N} \boldsymbol{H}(\boldsymbol{X} - \boldsymbol{X}_J)\boldsymbol{H}(\boldsymbol{X} - \boldsymbol{X}_J)^T \Phi_{a_J}(\boldsymbol{X} - \boldsymbol{X}_J)\Delta W_J \tag{4}$$

The window function Φ_a has a finite support size that is controlled by the dilation parameter a. Therefore, the sum in Equation 4 does not need to be performed for all particles $\boldsymbol{X}_J$; only those particles whose support covers $\boldsymbol{X}$ are involved in the computation. Consequently, Equation 4 can be rewritten as

$$\boldsymbol{M}(\boldsymbol{X}) = \sum_{J \in P(X)} \boldsymbol{H}(\boldsymbol{X} - \boldsymbol{X}_J)\boldsymbol{H}(\boldsymbol{X} - \boldsymbol{X}_J)^T \Phi_{a_J}(\boldsymbol{X} - \boldsymbol{X}_J)\Delta W_J$$
$$P(\boldsymbol{X}) = \{J,\ \text{support } (\Phi_{a_J}) \text{ covers } \boldsymbol{X}\} \tag{5}$$

The space spanned by the shape functions in Equation 1 satisfy the reproducing conditions as defined by Liu [12], which are that this space contains all polynomials up to degree n. A Galerkin procedure is devised using the finite dimensional space spanned by the meshfree shape functions. Displacement variable $\boldsymbol{u}$ is approximated at any point $\boldsymbol{X}$ in the physical domain as

$$\boldsymbol{u}(\boldsymbol{X}) \rightarrow u_h(\boldsymbol{X}) = \sum_{I=1}^{N} \Psi_I(\boldsymbol{X})\boldsymbol{d}_I \tag{6}$$

where the unknowns are the generalized displacement $\boldsymbol{d}_I$, which are associated with each shape function. It is important to note that meshfree shape functions do not possess the Kronecker delta property; thus, the imposition of essential boundary conditions is more difficult than with FEA. In this paper, the Lagrange multiplier method is used to impose such conditions.

To evaluate the integrals that appear in the weak formulation, an integration method is necessary over the physical domain. A background mesh is used for this purpose, as shown in Figure 1. This mesh, unlike the mesh for FEA, does not have to be connected, because its only purpose is to provide a non-overlapping decomposition of the domain into smaller, simpler domains, for which a Gauss integration rule can be used.

3. Variational Equations of Nonlinear Hyperelastic Structures

Consider the structural domain Ω whose boundary is composed of $\Gamma = S_f \cup S_u$ and $S_f \cap S_u = \emptyset$. The displacement value is prescribed on surface S_u, while the traction force is provided on surface S_f. In conjunction with the Lagrange multiplier method used to impose the essential boundary condition, the total potential energy of hyperelasticity in the mixed formulation is

$$\begin{aligned}\Pi(\boldsymbol{u}, \tilde{p}, \lambda^{S_u}) = &\int_{^0\Omega} W(\boldsymbol{u}, \tilde{p})\, d\Omega - \int_{^0\Omega} u_i f_i^B d\Omega \\ &- \int_{^0S_f} u_i f_i^{S_f} d\Gamma - \int_{^0S_u} \lambda_i^{S_u}(u_i - u_i^p) d\Gamma\end{aligned} \tag{7}$$

where $W(\boldsymbol{u}, \tilde{p})$ is the strain energy density function for the nearly incompressible hyperelastic material, $\tilde{p}$ is the hydrostatic pressure, $\boldsymbol{u}$ is the displacement vector, λ^{S_u} is the Lagrange multiplier associated with the essential boundary conditions, f^B is the externally applied body force, f^{S_f} is the surface traction, and u^p is the prescribed displacement on surface S_u. The reason for introducing the Lagrange multiplier is that the meshfree interpolation function in Equation (1) does not pose a Kronecker delta property on the essential boundary.

First, by applying the stationary condition of the total potential energy, and then by linearizing the variational equation, the incremental system of equations can be written in as

$$a^*({}^t z; \Delta z, \bar{z}) = \ell(\bar{z}) - a({}^t z, \bar{z}), \quad \forall \bar{z} \in Z \tag{8}$$

where the unknown variables are collected in $\mathbf{z} = \{\boldsymbol{u}, \lambda^{S_u}, \tilde{p}\}$, Δz is the increment of z, and $\bar{z}$ is the variation of z. The left superscript t denotes the configuration time, and the overbar "–" represents the quantity's first–order variation. In Equation (8), $a^*({}^t \boldsymbol{z}; \cdot, \cdot)$ is an energy bilinear form, $a(\cdot, \cdot)$ is an energy nonlinear form, and $(\cdot)$ is a load linear form. The detailed derivations of these forms can be found in [13]. For the purposes of completeness, only the final expression of these forms have been presented as follows:

$$\begin{aligned}a({}^t \boldsymbol{z}, \boldsymbol{z}) = &\int_{^0\Omega} {}^t S_{ij} \bar{\varepsilon}_{ij}\, d\Omega + \int_{^0\Omega} \bar{\tilde{p}}({}^t J - 1 - {}^t \tilde{p}/k)\, d\Omega \\ &- \int_{^0S_u} {}^t \lambda_i^{S_u} \bar{u}_i^{S_u}\, d\Gamma - \int_{^0S_u} \bar{\lambda}_i^{S_u}({}^t u_i^{S_u} - {}^t u_i^p)\, d\Gamma\end{aligned} \tag{9}$$

$$\ell(\bar{z}) = \int_{^0\Omega} \bar{u}_i {}^t f_i^B d\Omega + \int_{^0S_f} \bar{u}_i {}^t f_i^{S_f} d\Gamma \tag{10}$$

$$\begin{aligned}a^*({}^t \boldsymbol{z}; \Delta \boldsymbol{z}, \bar{\boldsymbol{z}}) = &\int_{^0\Omega} D_{ijkl} \bar{\varepsilon}_{ij} \Delta \varepsilon_{kl}\, d\Omega + \int_{^0\Omega} {}^t S_{ij} \Delta \bar{\eta}_{ij}\, d\Omega \\ &+ \int_{^0\Omega} {}^t J_{,\varepsilon_{ij}} \bar{\varepsilon}_{ij} \Delta \tilde{p}\, d\Omega \\ &+ \int_{^0\Omega} \bar{\tilde{p}}({}^t J_{,\varepsilon_{ij}} \Delta \varepsilon_{ij} - \Delta \tilde{p}/k)\, d\Omega \\ &- \int_{^0S_u} (\Delta \lambda_i^{S_u} \bar{u}_i^{S_u} + \bar{\lambda}_i^{S_u} \Delta u_i^{S_u})\, d\Gamma\end{aligned} \tag{11}$$

In Equations (9)–(11), S_{ij} is the second Piola–Kirchhoff stress, ε_{ij} is the Green–Lagrangian strain, η_{ij} is the nonlinear strain, D_{ijkl} is the fourth-order material tensor, J is the determinant of the deformation gradient, and k is the bulk modulus.

The linear, incremental expression in Equation 8 is discretized using the meshfree method discussed in the previous section. For highly nonlinear problems, the load is applied in several steps, and the iterative procedure in Equation (8) is needed to find a solution for each load step.

4. Shape Design Sensitivity Analysis of a Hyperelastic Structure

In shape design optimization, the geometry of the structure changes during the design process. Choi and Haug [14] have divided the process into two stages for obtaining the shape design sensitivity. First, the influence of the shape design variable on the physical domain is taken into account using the design velocity concept. Second, the shape design sensitivity coefficient is computed using the material derivative concept from continuum mechanics. Shape design sensitivity for nonlinear structures has been reviewed and summarized by Choi [15].

The sensitivity equation can be obtained by taking the material derivative of the equilibrium Equation 8 at the final load step for each design variable as

$$a^*({}^t\mathbf{z}; {}^t\dot{\mathbf{z}}, \bar{\mathbf{z}}) = a'_V({}^t\mathbf{z}, \bar{\mathbf{z}}) + \ell'_V(\bar{\mathbf{z}}), \quad \forall \bar{\mathbf{z}} \in Z \tag{12}$$

where

$$\begin{aligned} &a'_V({}^t\mathbf{z},\bar{\mathbf{z}}) \\ &= \int_{{}^0\Omega} (D_{ijkl}\bar{\varepsilon}_{ij}\varepsilon^V_{kl} + D_{ijkl}\bar{\varepsilon}^V_{ij}\varepsilon_{kl} + {}^tS_{ij}\bar{\eta}^V_{ij} + {}^tS_{ij}\bar{\varepsilon}_{ij} div\boldsymbol{V})d\Omega \\ &\quad + \int_{{}^0\Omega} \bar{\tilde{p}}[{}^tJ_{,\varepsilon_{ij}}\varepsilon^V_{ij} + ({}^tJ - 1 - \tilde{p}/k)div\boldsymbol{V}]d\Omega \end{aligned} \tag{13}$$

$$\begin{aligned} \ell'_V(\bar{\mathbf{z}}) &= \int_{{}^0\Omega} \bar{u}_{i0}\nabla^t f^B_i d\Omega + \int_{{}^0\Omega} \bar{u}_i{}^t f^B_i div\boldsymbol{V}\, d\Omega \\ &\quad + \int_{{}^0S_f} \bar{u}_i 0\nabla^t f^{S_f}_i d\Gamma + \int_{{}^0S_f} \bar{u}^t_i f^{S_f}_i \kappa d\Gamma \end{aligned} \tag{14}$$

In Equation 13, strain terms ε^V_{ij}, $\bar{\varepsilon}^V_{ij}$, and $\bar{\eta}^V_{ij}$ are explicitly dependent on the design velocity, for which expressions can be found in [13]. In Equation 14, the applied loads are presumed to be conservative; thus, they are independent of the design velocity.

For the hyperelastic structure, the same bilinear form that appeared in Equation 8 also appears on the left side of Equation 12. This fact offers an important computational advantage, since the last stiffness matrix that was factorized at the analysis stage in Equation 8 can be reused for solving the design sensitivity equation. After solving for $\dot{\mathbf{z}}$, the sensitivity coefficient of a performance measure can be obtained by using the chain rule of differentiation.

5. CAD-Based Optimization Procedure

The integration of the CAD tool, meshfree analysis tool, and DSA and optimization tool is illustrated in Figure 2. The discrete model is constructed using the

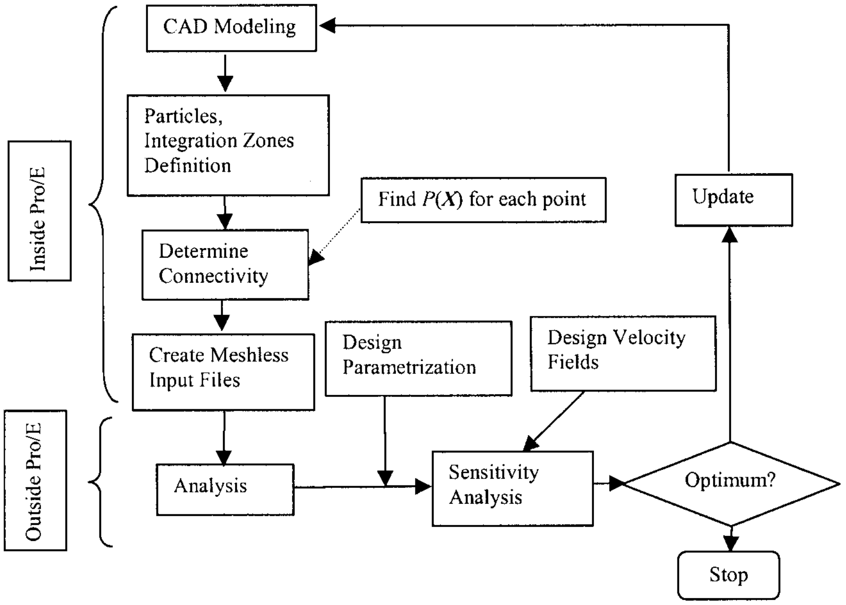

Figure 2. CAD-meshfree analysis–optimization flowchart.

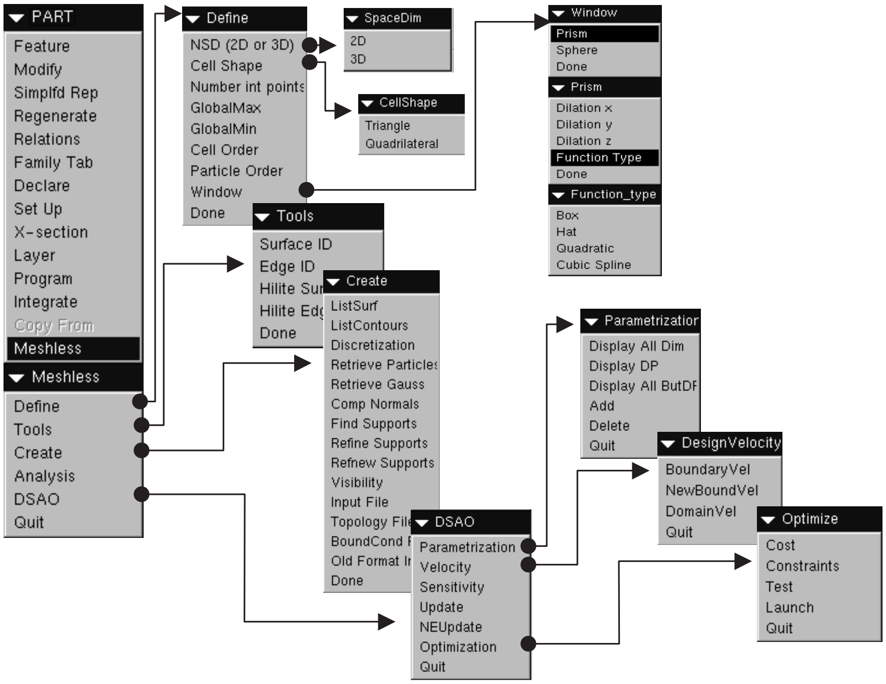

Figure 3. CAD integrated menu organization.

built-in capabilities of Pro/ENGINEER that were originally developed for the finite element method. Pro/ENGINEER provides access to a model database through a set of functions organized in Pro/TOOLKIT and Pro/DEVELOP libraries. These libraries allow users to add functionality to Pro/ENGINEER, and to seamlessly integrate the resulting application. The Graphical User Interface is developed under a Pro/ENGINEER cascade menu system, as shown in Figure 3. The meshfree module is launched within Pro/ENGINEER as a separate application. The definition of the meshfree model can be made using the cascading menus developed for seamless integration.

CAD-based shape design parameterization identifies CAD parameters as design variables for shape DSA and optimization. In a dimension-driven CAD tool such as Pro/ENGINEER the design engineer can capture design intent in the model. Because dimensions that define the CAD model change during the optimization process, the model can be updated automatically. For a consistent and stable optimization, cost and constraints need to be defined with respect to those same particles in the initial design. It is therefore necessary to update the discrete model in a way that is consistent with the updated CAD model. The particles that were on a particular edge or surface of the initial design must remain on that same edge or surface of the updated design, although the shapes of the edges and surfaces themselves may change.

To achieve an accurate computation of design sensitivity coefficients, a reliable and efficient method to determine the design velocity fields is essential. It is difficult to compute the velocity fields analytically with a general CAD model. In this paper, a new hybrid method is proposed that is based on finite difference and boundary displacement procedures and that overcomes the difficulties experienced by Hardee et al. [3].

For this proposed method, a design velocity field associated with a shape design variable is computed for any point in the CAD model. Denoting T as the transformation corresponding to a design variable τ, the velocity field is

$$\boldsymbol{V}({}^0\boldsymbol{x}_\tau, \tau) \equiv \frac{d\,{}^0\boldsymbol{x}_\tau}{d\tau} = \frac{d\boldsymbol{T}({}^0\boldsymbol{x}_\tau, \tau)}{d\tau} = \frac{\partial \boldsymbol{T}({}^0\boldsymbol{x}_\tau, \tau)}{\partial \tau} \tag{15}$$

The velocity at point A is calculated using the finite difference method as

$$\boldsymbol{V}_A = ({}^0\boldsymbol{x}_A^{\text{pert}} - {}^0\boldsymbol{x}_A)/\delta\tau \tag{16}$$

In the finite difference approach, the smallest possible step size $\delta\tau$ has to be selected, although it cannot be so small that there is numerical error. A further difficulty in applying this method is that it is not easy to determine the position of point A in the perturbed model (${}^0\boldsymbol{x}_A^{\text{pert}}$), as it corresponds to the initial position ${}^0\boldsymbol{x}_A$. This is the same previously discussed problem of starting with an initial discrete model that is consistent with the CAD model, and then locating a discrete model that corresponds to the updated (or perturbed) CAD model. If another automatic discretization procedure is used, as with the building of the initial meshfree model, then the process will create a different number of particles in general, and it will be impossible to obtain a mapping from the initial to the new particles. A hierarchical boundary displacement method is proposed, and is discussed in the following section.

6. The Hierarchical Boundary Displacement Method

One of the most important procedures of design optimization is the model update procedure. Most modern CAD tools allow the design engineer to obtain a new design by changing key parameter values. As noted earlier, the problem is how to update the discrete model. The approach proposed here assumes that the CAD tool uses a surface modeling technique and that the geometric representation of curves and surfaces is available via API. Because only the boundary geometry is represented by the CAD tool, the particles on the boundary are the first to be updated.

A hierarchical boundary displacement method follows the geometric hierarchy of the CAD model: a general part is a boundary-represented solid, and each surface on the boundary is a parametric surface trimmed by one external contour and, possibly, several internal contours. Each contour is formed by edges, which have a simple 1D parameterization.

The method follows the hierarchy of the geometry, starting from the particles on the edges, continuing to the particles on the boundary surfaces, and finally, moving to the particles on the interior of the solid model. The particles on the edges are updated using a 1D parametrization, as explained in Figure 4(a). The parametric position t_A of particle A in the initial design, and retrieved using API, is used to compute the corresponding position of the particle A'.

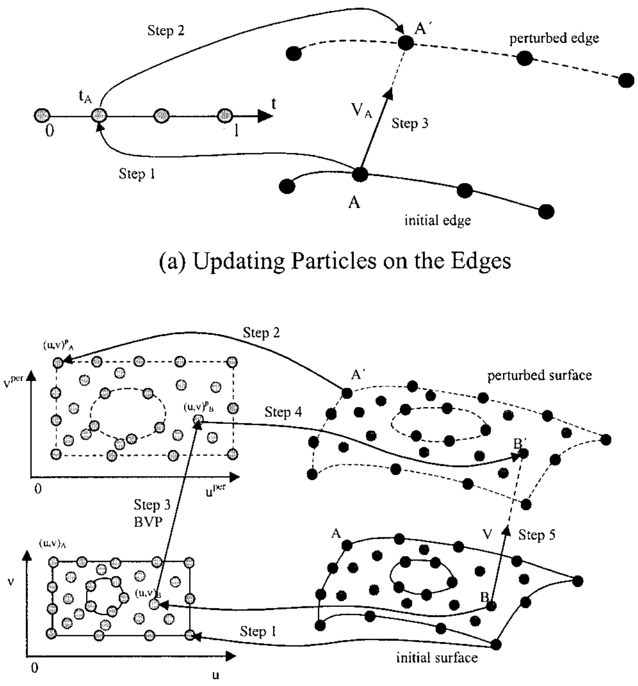

(a) Updating Particles on the Edges

(b) Updating Particles on the Boundary Surfaces

Figure 4. CAD-based update for particles on the edges and boundary surfaces.

For those particles that are on boundary surfaces but not on edges, a 2D boundary displacement method is used, as explained in Figure 4(b). First, the two-parameter position (u,v) is obtained for all initial design particles using API. Next, the two-parameter position $(u,v)^{\text{pert}}$ is retrieved for all particles on the edges of the perturbed surface. Further, a 2D boundary value problem is solved in the parametric space (u,v), in order to find the parametric position corresponding to particles on the interior of the surface. The algorithm for computing the design velocity fields is given below. This method is implemented using the functions available in the Pro/TOOLKIT library.

1. Using API, retrieve the parameter $(u,v)_{S,P}$ for each surface S, for each particle P on surface S, and retrieve the parameter $t_{E,Q}$ for each edge E, for each particle Q on edge E. Parameter t is always between 0 and 1 (Step 1 in Figure 4).
2. Using a small design perturbation δd, regenerate the CAD model to obtain the perturbed model.
3. Calculate the new position of particle Q on edge E on the perturbed model, using the parameter $t_{E,Q}$ (Step 2).
4. For each face (trimmed surface) of the perturbed model:
    (a) Find the new parameters $(u,v)^{\text{pert}}$ for all the particles on the edges.
    (b) Solve the boundary value problem in space (u,v), to find $(u,v)^{\text{pert}}$ for all particles on the interior of the surface that are not on the edges (Step 3).
    (c) Find new positions of all particles on the surface, using the corresponding $(u,v)^{\text{pert}}$ (Step 4).
    (d) Compute the velocity for all particles on the boundary (Step 5).
5. Repeat Steps 2–4 for each design variable.

Once the parametric position has been obtained, the actual position can be found for any particle on the updated surface using API. This method ensures that particles on the surface of the initial design will remain on the surface of the updated design. If a boundary displacement method has been directly applied to the general 3D surface, then the above consistency cannot be guaranteed.

Next, a 3D boundary displacement method is used to find the updated position of particles on the interior of the solid model during the initial design. To this end, a 3D boundary value problem is solved for all shape design parameters at the same time, using the Lagrange multiplier method. Only one factorization of the augmented stiffness matrix is required, and only forward and backward substitutions are necessary for the design velocity computation of each shape design parameter.

7. CAD-Based Optimization of an Engine Mount

In order to illustrate the proposed methodology, half of an engine mount with imposed displacement boundary conditions is modeled, as shown in Figure 5(a). The engine mount is composed of an outer metal casing attached to the car body, an inner metal piece connected to the engine, and intermediary rubber material to provide appropriate stiffness and compliance to isolate engine vibration. The interior metal block is treated as a rigid body, and the stiffness of the mount is selected as a performance measure. The exterior casing is considered fixed. Stiffness is determined by calculating the ratio between the reaction force and the imposed displacement in the final load step. The hydrostatic pressures at critical points are also selected as performance measures.

The engine mount particle model and integration zone model is created using Pro/ENGINEER's FEA functions. The model has 361 particles and 218 integration zones, as shown in Figure 5(b). The displacements are prescribed on the particles located at the interface between the rubber and interior metal block. The interface particles are pushed downward (with lateral movement restrained) to a displacement of 13.79 mm, which is the distance between the inner metal block and the lower rubber bumper. The Mooney-Rivlin material model is employed to describe the hyperelastic behavior, with material constants $A_{10} = 0.145\,\text{MPa}$, $A_{01} = 0.062\,\text{MPa}$, and bulk modulus $k = 10{,}000\,\text{MPa}$, to enforce the nearly incompressible condition.

The meshfree analysis is carried out in 25 load steps, due to the high nonlinearity of the model and the large deformation. Figure 5(c) shows the fringe plot of the hydrostatic pressure on the deformed structure. This hydrostatic pressure is interpolated separately from the displacements, and it is assumed to be constant over an integration zone. It is condensed at the integration zone level.

Eighteen shape design parameters are selected for this problem: the x- and y-coordinates of the nine datum points on the boundary, as shown in Figure 5(a). These datum points control the shape of the engine mount's interior boundary. Eighteen corresponding design velocity fields are computed using the method explained in previous sections. The shape design velocity field corresponding to design parameter d_{67} is plotted using the vector plot in Figure 5(d).

After the meshfree analysis converges to the final load step, design sensitivity analysis is carried out once using the factorized tangent stiffness matrix. Table 1 shows the sensitivity results of various performance measures with respect to design variable d_{76}. In order to verify the accuracy of the design sensitivity coefficients, the forward finite difference method is employed with a perturbation of 0.01 mm for design variable d_{76}. Excellent agreements between the continuum-based sensitivity and finite difference results are obtained in the last column of the table.

Design optimization of the engine mount is carried out using the design optimization tool. The structure's

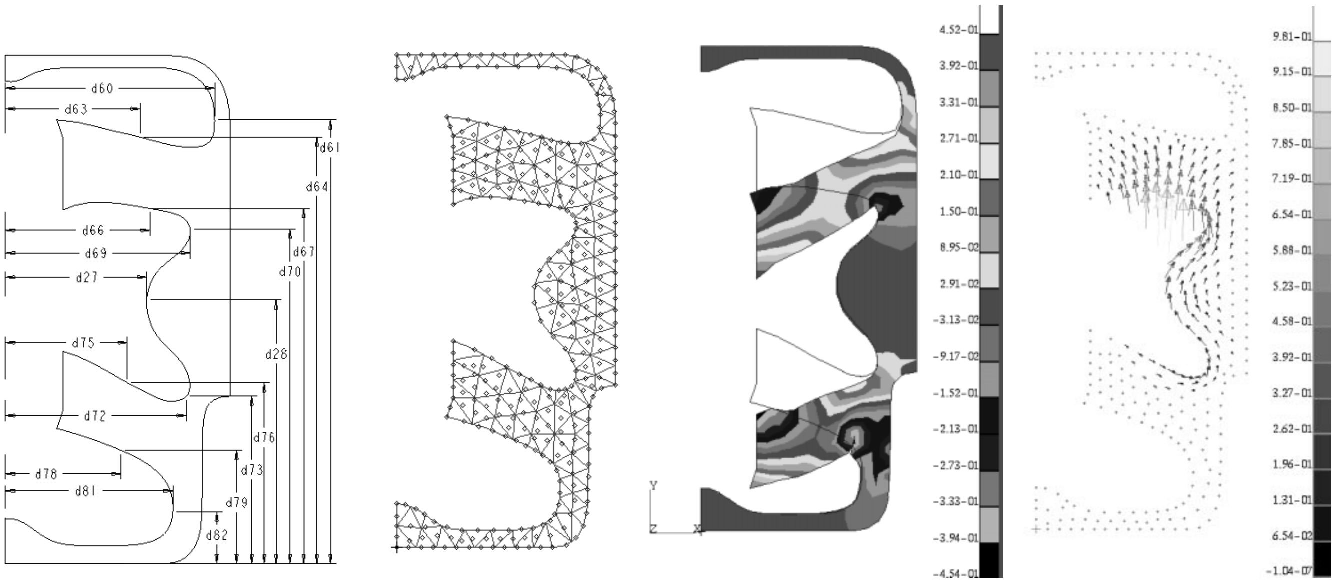

(a) CAD Model (b) Discretization (c) Analysis Results (d) Design Velocity

Figure 5. An engine mount example.

area is selected as the object function. Two types of constraints are considered: the hydrostatic pressure and stiffness. The pressure should be within an acceptable limit at the final design stage. It is also important that the stiffness of the engine mount, defined as the ratio between resistance force and maximum displacement, be maintained at the same level with the initial design.

The values for object and constraint functions are provided from the meshfree analysis results, and the gradients for these functions are computed from DSA. Velocity fields are obtained every time the optimization algorithm requests sensitivity information. The position of the particles is updated following the same procedure used in the computation of the velocity field. The integration model is changed at each design iteration using API, and a meshfree model that is consistent with the CAD model is generated at each design iteration.

The design optimization problem converges after six iterations. Optimization histories (cost, design variables and normalized constraints) are shown in Figure 6(a), the meshfree model at the optimum design is shown in Figure 6(b), and the hydrostatic pressure plot on a deformed structure is shown in Figure 6(c). Table 2 compares the initial and optimum design. About 16% of the initial material is reduced in the optimum design, while maintaining the same mechanical performance. Load–deflection curves at the initial and optimum design are shown in Figure 7, where it is

Table 1. Design sensitivity verification for engine mount model.

Performance Measure	Initial Value	Perturbed Value*	Sensitivity Coefficient	Verification
Pressure, particle 7	– 0.4542325E + 0	– 0.4547694E + 0	– 0.5381110E – 1	99.78
Pressure, zone 146	– 0.3512860E + 0	– 0.351394E + 0	– 0.1090690E – 1	99.20
Total reaction force	– 0.3032391E + 1	– 0.3033125E + 1	– 0.7351846E – 1	99.92
Total volume	– 0.1073783E + 4	– 0.1073874E + 4	– 0.9061015E + 1	100.00
y-displ., at particle 59	– 0.7765927E + 0	– 0.7766633E + 0	– 0.7056031E – 2	100.06

*perturbation 0.01 mm for design variable d_{76}

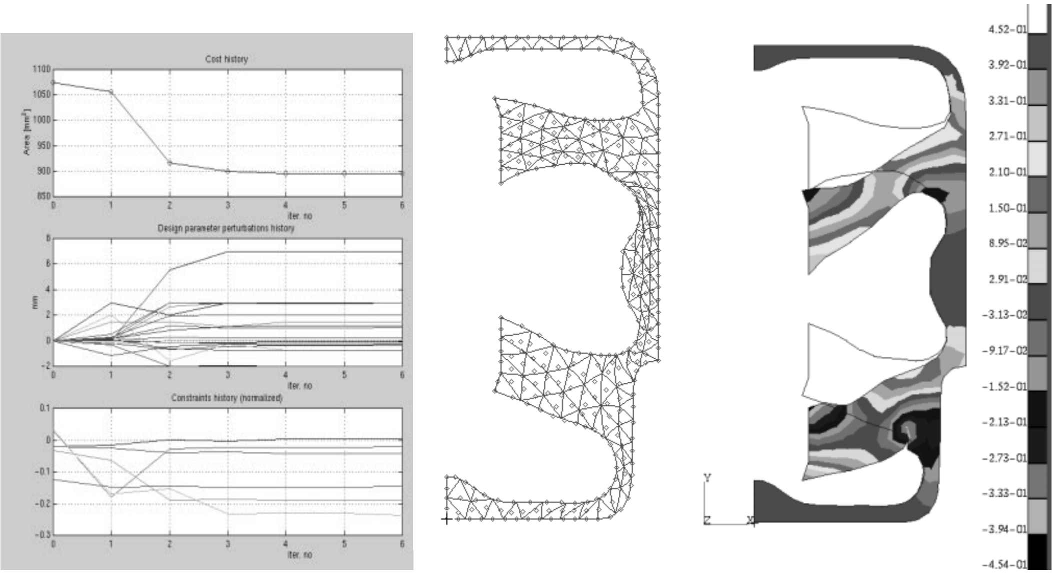

(a) Optimization History (b) Optimum Geometry (c) Analysis Results at Optimum

Figure 6. Design optimization results.

Table 2. Design optimization results of engine mount model.

Performance Measure	Initial Design	Optimum Design	Absolute Change	Relative Change [%]
Total area (cost)	1073.7833	894.7004	– 179.0829	16.67
Total reaction force	– 3.032390	– 2.9647224	0.06767	2.23
Pressure, particle 7	– 0.4542325	– 0.4307406	0.0235	5.17
Pressure, zone 146	– 0.3512860	– 0.4200193	0.06873	19.56

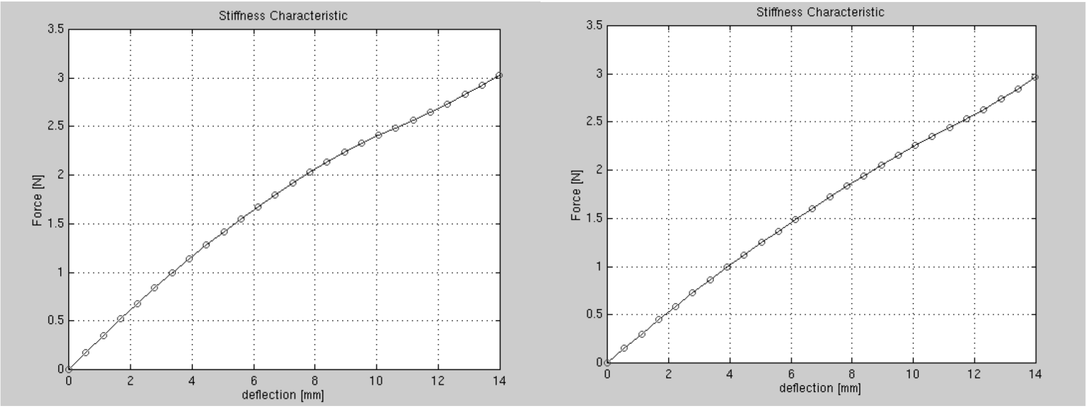

(a) Initial Design

(b) Optimum Design

Figure 7. Load–deflection curve.

evident that mechanical characteristics are nearly identical.

8. CAD-Based Optimization of an Elastic Beam

Even though design optimization of the nonlinear problem has been carried out in the above 2D example, a major advantage of CAD-based optimization appears in the 3D design problem, which is the purpose of this section. A variable-section beam is modeled as a 3D problem, as shown in Figure 8(a). The CAD model consists of general blend protrusions and cross sections with I-shape.

Two cut features are made in order to minimize the amount of material used. The beam is simply supported at both ends, and a uniform pressure is applied in the vertical direction.

Because the geometry and applied load are symmetric, only a quarter of the model is analyzed. The discrete model is shown in Figure 8(b). This model contains 817 particles, and 1548 10-node tetrahedrons that are used as integration zones. A total of 2842 nodes are used to describe the tetrahedrons. The global distance between particles in this model is 15 mm, and the support size is set to 20 mm in each direction, ensuring that every point in the model is covered with at least four particle supports that are not on the same plane. The integration model has a global size of 20 mm, and is more refined near the cut feature. Young's modulus is $E = 21000\,\mathrm{N/mm^2}$ and Poisson's ratio is $\nu = 0.3$. The von Mises stress plot on the deformed shape is shown in Figure 8(c). With a total force of 4000 N, a maximum displacement of 0.0018 mm appears at particle 689, and the maximum von Mises stress of 4.26 MPa appears at particle 79.

To achieve shape design optimization, thirteen design variables are selected, as shown in Figure 9(a). There are nine parameterized sections, but because of symmetry, only five are independent. Each section has two variable dimensions: d_1 and d_6 for section 1, d_{13} and d_{16} for section 2, d_{20} and d_{22} for section 3, d_{27} and d_{29} for section 4, and d_{34} and d_{36} for section 5. The cut feature is controlled by three parameters, d_{50}, d_{51} and d_{52}, which define the length of the cut, the radius of the arc, and the distance between the center of the cut and the end of the beam.

Shape design velocity fields corresponding to these design variables are computed using the previously discussed method. The vector plot corresponding to design d_{51} is shown in Figure 9(b), illustrating how design parameter changes affect the CAD model and the discrete model.

The volume of the beam is selected as the object function. Two types of constraints are considered: vertical displacement of the beam's middle section and maximum von Mises stress developed at the simply supported ends. The maximum von Mises stress should not exceed 5.0 MPa, and the maximum displacement allowed is 0.0035 mm.

The design optimization converges in seven iterations. The meshfree model and von Mises stress on a deformed structure at optimum design is shown in Figure 10. The volume of the beam was reduced from 824,064 mm^3 to 543,699 mm^3, while maintaining the maximum displacement at 0.0035 mm and the maximum von Mises stress at 5.0 MPa.

The optimum CAD model is compared to the initial model in Figure 11. At the initial design stage, all constraints were satisfied; at the optimum design, displacement constraints became active in the middle section. The beam's volume decreases by increasing the length and the radius of the cut features, and by reducing the width of the five parameterized sections. It is interesting to note that the third section has a bigger width value than the second or fourth section. This can be explained by the presence of the hole, which weakened the beam primarily in the third section.

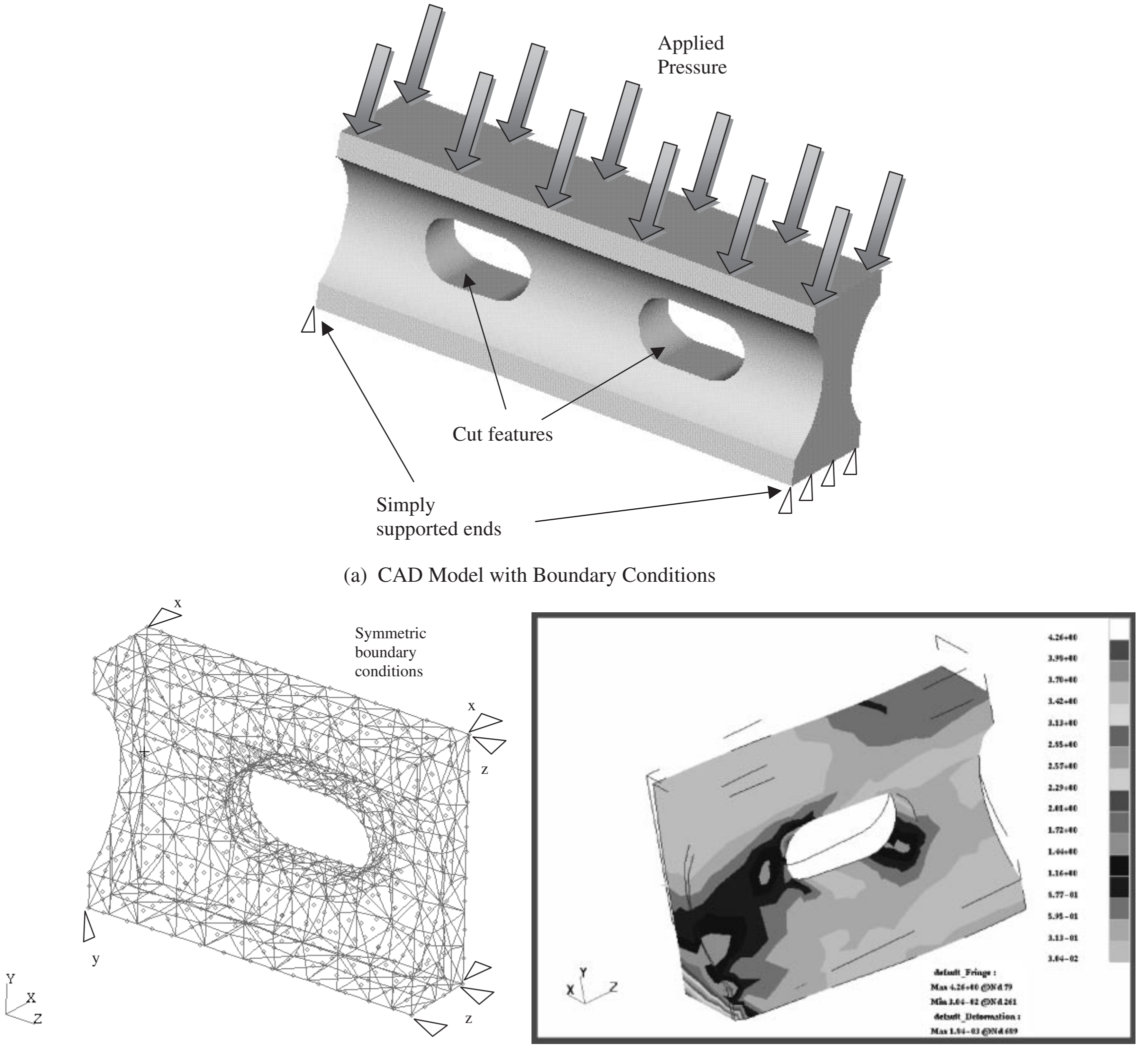

(a) CAD Model with Boundary Conditions

(b) Discrete Meshfree Model

(c) Stress Contour Plot

Figure 8. 3D beam CAD model and meshfree analysis results.

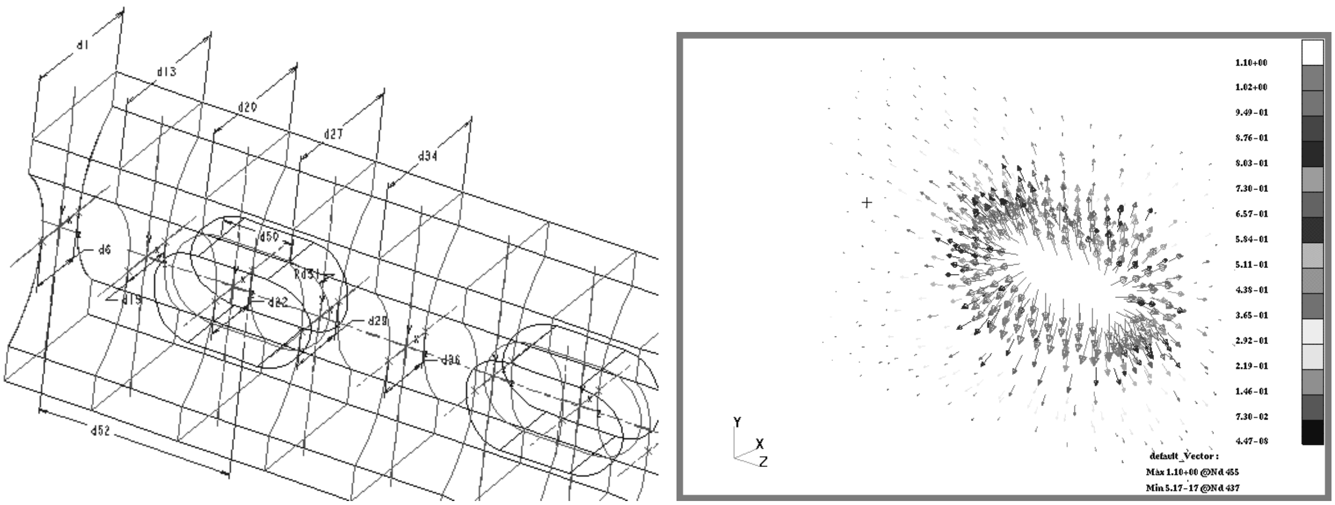

(a) CAD-Based Design Parameters

(b) Design Velocity Field

Figure 9. Beam parametrization and design velocity field plot.

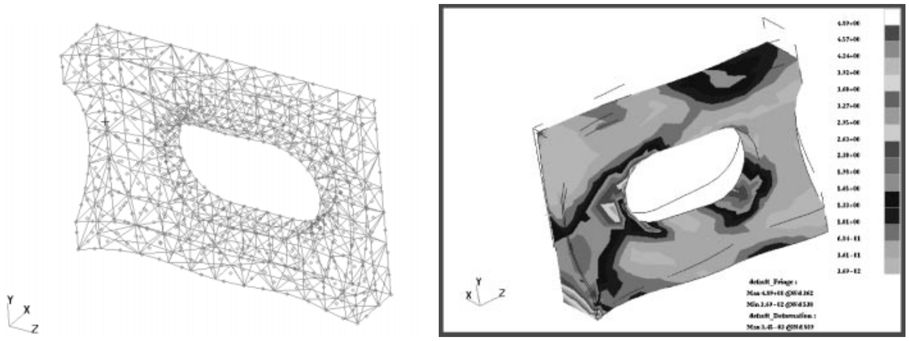

(a) Meshfree Model at Optimum Design

(b) Stress Contours at Optimum Design

Figure 10. Meshfree model and analysis results at optimum design.

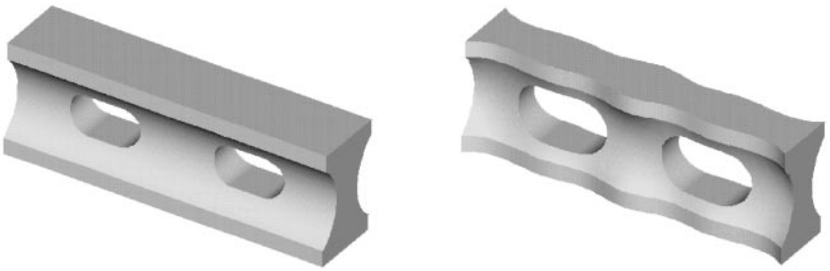

(a) CAD Model at Initial Design

(b) CAD Model at Optimum Design

Figure 11. The CAD model at initial and optimum designs.

9. Conclusions

CAD-based shape design sensitivity and optimization methods using a meshfree method were presented. The proposed approach is quite general and can be applied to large deformation problems and to important modifications in the design. The method proved to be effective for optimization using the examples of an engine mount and an elastic beam.

Shape DSA and optimization using the meshfree method holds great potential for eliminating mesh distortion problems that occur when the traditional finite element method is used. Currently, such research is being extended to 3D elasto-plastic problems, and contact problems, demonstrating the advantages of applying meshfree design to support CAD-based shape optimization.

ACKNOWLEDGMENTS

This research was supported by NSF/DARPA Optimized Portable Algorithms and Application Libraries (OPAAL) Program. This support is gratefully acknowledged.

References

1. *Pro/ENGINEER User's Guides, version 20*. (1999). Parametric Technology Corporation, 128 Technology Drive, Waltham, MA 02154.
2. Yang, R.J. and Fiedler, M.J. (1987). Design modeling for large-scale three-dimensional shape optimization problems. *Proceedings of the 1987 ASME International Computers in Engineering Conference and Exhibition*. New York, NY. pp. 177–182.
3. Hardee, E., Chang, K.-H, Tu, J., Choi, K.K., Grindeanu, I. and Yu, X. (1999). A CAD-based design parameterization of elastic solids. *Advances in Engineering Software*, **30**: 185–199.
4. Chang, K.H. and Choi, K.K. (1992). A geometry based shape design parameterization method for elastic solids. *Mech. Struct. Machines*, **20**(2): 215–252.
5. Chang, K.H., Choi, K.K., Tsai, C.S., Chen, C.J., Choi, B.S. and Yu, X. (1995). Design sensitivity analysis and optimization tool (DSO) for shape design applications. *Computing Systems in Engineering*, **6**(2): 151–175.
6. Choi, K.K. and Duan, W. (2000). Design sensitivity analysis and shape optimization of structural component with hyperelastic material. *Comp. Meth. Appl. Mech. Eng.*, **187**(1–2): 219–243.
7. Yao, T.M. and Choi, K.K. (1989). 3D shape optimal design and automatic finite element regridding. *Int. J. Num. Meth. Eng.*, **28**(2): 369–384.
8. Belegundu, A.D. and Rajan, S.D. (1988). A shape optimization approach based on natural design variables and shape functions. *Comp. Meth. Appl. Mech. Eng.*, **66**: 87–106.
9. Rajan, S.D. and Belegundu, A.D. (1989). Shape optimization using fictitious loads. *AIAA Journal*, **27**(1): 102–107.
10. Choi, K.K. and Chang, K.H. (1994). A study on velocity field computation for shape design optimization. *Finite Elements in Analysis and Design*, **15**: 317–341.

11. Belytschko, T., Krongauz, Y., Organ, M., Flemming, D. and Krysl, P. (1996). Meshless methods: an overview and recent developments. *Comp. Meth. Appl. Mech. Eng.*, **139**(1–4): 3–47.
12. Liu, W.K., Jun, S. and Zhang, Y.F. (1995). Reproducing kernel particle methods. *Int. J. Num. Meth. Eng. in Fluids*, **20**: 1655–1679.
13. Grindeanu, I., Chang, K.-H, Choi, K.K. and Chen, J.S. (1998). Design sensitivity analysis of hyperelastic structures using a meshfree method. *AIAA Journal*, **36**(8): 618–627.
14. Choi, K.K. and Haug, E.J. (1983). Shape design sensitivity analysis of elastic structures. *J. of Structural Mechanics* **11**(2): 231−269.
15. Choi, K.K. (1993). Design sensitivity analysis of nonlinear structures II. In: Kamat, M.P. (ed.) *Structural Optimization: Status and Promise*, Chapter 16, Progress in Astronautics and Aeronautics, AIAA, pp. 407–446.

Iulian Grindeanu

Iulian Grindeanu is currently a development engineer in the CAE Division of the LMS INTERNATIONAL. He graduated with a Ph.D. in the Department of Mechanical Engineering from the University of Iowa in 1999. His research areas are design optimization, design sensitivity analysis, meshfree methods, CAE-CAD integration, and automatic mesh generation. He has published six journal papers in the above areas. He can be reached at iulian@lmscae.com.

Nam Ho Kim

Nam Ho Kim is currently an assistant professor at the Department of Mechanical Engineering in the University of Florida. He graduated with a Ph.D. in the Department of Mechanical Engineering from the University of Iowa in 1999. His research area is design optimization, design sensitivity analysis, nonlinear structural mechanics, structural acoustics, and meshfree method. He has published more than twenty refereed journal and conference papers in the above areas. He can be reached at nkim@ufl.edu.

Kyung K. Choi

Kyung K. Choi is currently a professor at the Department of Mechanical and Industrial Engineering in the University of Iowa. He is also Director of Center for Computer Aided Design. He is a fellow of ASME and associate fellow of AIAA. He graduated with a Ph.D. in the Department of Mechanical Engineering from the University of Iowa in 1980. His research area is mechanical system design sensitivity analysis and optimization, reliability-based design optimization, computational methods in mechanics, integration of CAE tools for concurrent engineering. Author and co-author of 180 technical papers and three books. He can be reached at kkchoi@ccad.uiowa.edu.

J.S. Chen

J.S. Chen is currently an Associate Professor at the Department of Civil & Environmental Engineering, University of California, Los Angeles. He received Ph.D. from Theoretical & Applied Mechanics of Northwestern University in 1989. His research interests are in finite element and meshfree methods for nonlinear mechanics problems with large deformation, strain localization, and moving interfaces for applications to rubber materials, metal forming processes, geotechnical materials, materials science, and nanomechanics. He has published more than 100 journal and conference papers. He can be reached at jschen@seas.ucla.edu.